International Journal of Thermal Sciences 49 (2010) 1253–1263

Contents lists available at ScienceDirect

International Journal of Thermal Sciences

journal homepage: www.elsevier.com/locate/ijts

Pressure drop across micro-pin heat sinks under unstable boiling conditions

Ali Koşar [a,*], Mehmed Rafet Özdemir [a], Mehmet Keskinoz [b]

[a] Sabancı University, Faculty of Engineering and Natural Sciences, Mechatronics Engineering Program, Orhanlı, Tuzla 34956, Istanbul, Turkey
[b] Sabancı University, Faculty of Engineering and Natural Sciences, Electronics Engineering Program, Orhanlı, Tuzla 34956, Istanbul, Turkey

ARTICLE INFO

Article history:
Received 29 July 2009
Received in revised form
22 December 2009
Accepted 25 December 2009
Available online 26 February 2010

Keywords:
Micro pin fins
Microchannels
Unstable boiling
Boiling instabilities

ABSTRACT

Flow boiling was investigated under unstable boiling conditions in three different micro-pin fin heat sinks using water and R-123 as working fluids. Once boiling was initiated severe temperature fluctuations were recorded for all the tested (three) micro-pin fin heat sinks.

Flow images and fast-Fourier transform (FFT) of pressure signals during flow boiling were used to explain experimental results. The boiling instability mechanisms behind unstable boiling were discussed for both water and R-123. Accordingly, no significant pressure fluctuations with respect to time averaged pressure drop were evident for the tested micro-pin fin heat sinks before and after flow boiling instability initiates. However, a step change in the pressure signals were recorded with the inception of unstable boiling, and a sharp increase in the magnitude peaks of the FFT profiles was observed in the device operated with R-123, while there was no significant change in the FFT profiles in the devices operated with water. According to complementary flow visualization studies, the oscillation frequency of the periodic flow patterns for the device operated with R-123 was higher ($f \sim 80$ Hz) than that of the devices operated with water ($f \sim 20$ Hz).

1. Introduction

Driven by the continuous demand for aggressive thermal management solutions, heat and fluid flow in microchannels has been extensively studied in the last decade. Summaries of research efforts on this subject are available in recent literature reviews [1–7].

To provide superior heat transfer performance in microscale cooling applications, heat transfer area enhancement methods using micro-pin fins have been recently explored [8–20]. High heat removal rates were achieved in flow boiling due to the increase in active nucleation sites in addition to heat transfer area enhancement with micro-pin fins and lower increase in surface temperature with applied heat flux with boiling. However, the advantages of boiling heat transfer in micro-pin fin heat sinks could not be exploited unless micro heat sinks are carefully designed. Boiling instabilities leading to severe flow reversals, pressure oscillations and temperature fluctuations, which might cause premature critical heat flux (CHF), were reported for some microchannel configurations [4,11,21–23].

Bergles and Kandlikar [6] reviewed basic CHF mechanisms in microchannels in an extensive review. They emphasized on inlet restriction and presented it as the cure for both parallel channel and excursive type instabilities in parallel microchannels. In parallel lines, Koşar et al. [23] investigated the effect of the inlet orifice length on the suppression of boiling instabilities. They observed severe temperature and pressure fluctuations once boiling was incepted. This was the case when their configuration had no inlet micro orifice. They could obtain stable boiling data with the use of inlet micro orifices, and they showed whether the length of inlet orifice was sufficiently long boiling instabilities could be completely suppressed. Kandlikar et al. [22] could also stabilize flow boiling using inlet restriction. In addition, they could moderate boiling instabilities by including nucleated sites on microchannel walls. The suppression of boiling instabilities by such additional nucleation sites (by reentrant cavities) was also exploited by Kuo and Peles [24]. They recorded an extension of stable boiling region with reentrant cavities and could moderate rapid bubble growth, parallel channel and compressible volume instabilities, which were displayed as main boiling instability mechanisms in microchannels. In a later study of Kuo and Peles [25] on pressure effects on flow boiling instabilities, significant pressure effects on flow boiling instabilities in parallel microchannels were unveiled. Smaller bubbles recorded in visualization studies, the reduction of void fraction, and lower wall superheats needed for nucleation were held responsible for delays/suppression in compressible volume and rapid bubble growth instabilities.

In this study, unstable boiling caused by boiling instabilities in micro-pin fin heat sinks is investigated for the very first time to

* Corresponding author. Tel.: +90 216 483 9621; fax: +90 216 483 9550.
E-mail address: kosara@sabanciuniv.edu (A. Koşar).

1290-0729/$ – see front matter © 2010 Elsevier Masson SAS. All rights reserved.
doi:10.1016/j.ijthermalsci.2009.12.018

Nomenclature

Symbol	
d	chord thickness/pin fin diameter, m
f	frequency, s^{-1}
G	mass velocity based on the minimum cross sectional area, kg m^{-2} s^{-1}
H	height of the channel, m
k	index in Eqns. (1)–(4)
L	channel length, m
n	time index in Eqns. (1)–(2)
N	number of measurements in Eqn. (2)
p	pressure, kPa
P	electrical power, W
q''	heat flux, W cm^{-2}
S_L	longitudinal pitch, m
S_T	transverse pitch, m
w	channel width, m
t	time, s
T	temperature, °C
T_s	sampling period, s
$\overline{T}$	average surface temperature, °C
x	pressure drop, kPa
X	Fourier transform, s^{-1}
W	width of sampling window, s^{-1}

Greek	
Δp	pressure drop, kPa

Subscript	
max	maximum
p	peak
SAT	saturation

address to the lack of information about unstable boiling characteristics in the literature, where instability studies carried out so far were in plain microchannels. In this context, pressure drop characteristics and signals are obtained from three different micro-pin fin heat sinks so that a hydrodynamic approach is implemented to characterize unstable boiling phenomena in micro-pin fin heat sinks by processing the pressure drop signals along with the periodic appearance in flow patterns under unstable boiling conditions. In addition to this analysis, the results of the present study are compared to plain microchannel heat sinks results (exposed to boiling instabilities) so that valuable insight as regards unstable boiling phenomena in micro-pin fin heat sinks could be provided, and main differences from plain microchannels could be delineated. To accomplish this, three different micro-pin fin heat sinks are utilized under boiling conditions using two different working fluids (water, R-123). In the light of the literature about microchannels, configurations prone to boiling instabilities (low system pressure and without inlet restriction) are prepared to promote unstable boiling generated by boiling instabilities. Signal processing techniques (Discrete-Time Fourier Transform (DFT)) are employed to characterize the pressure fluctuations for immediately before and after the inception of unstable boiling and to associate them with boiling instabilities.

In summary, this study includes the presentation of the pressure drop data from three different micro-pin fin heat sink devices under unstable boiling conditions and detailed discussion about the cause and the characteristics of unstable boiling in these devices. First, a brief overview about the devices and experimental data will be presented. Subsequently, experimental procedure, data reduction, and signal processing technique will be covered. Finally, an extensive summary about the experimental results and major conclusions will be given.

2. Device overview

A Computer Aided Design (CAD) image of a representative device consisting of a 1800-μm wide and 1 cm long microchannel of depth 243-μm is shown in Fig. 1a. In order to minimize ambient heat losses an air gap is produced on the two ends of the side walls, and an inlet and exit plenum, 4 mm long each, are etched on the thin silicon substrate (~150 μm). A heater, which serves as a thermistor for temperature measurements, is deposited on the backside to deliver the heating power. A Pyrex cover seals the device from the top and allows flow visualization. Pressure taps are placed at the inlet and exit of the device to enable pressure measurements. A representative micro-pin fin heat sink is displayed in Fig. 1b. The devices which were tested in this study (Fig. 1b and c) are summarized in Table 1.

3. Experimental setup and procedure

3.1. Experimental setup

In Fig. 2, a schematic of the experimental setup is shown. The details about the experimental setup are included in the previous work of Koşar and Peles [11]. The micro-pin fin device was packaged by sandwiching it between two plates. The fluidic seals were forged using miniature "o-rings" while external electrical connections to the heater were provided from beneath through spring-loaded pins, which connected the heater to electrical pads residing away from the main micro-pin fin device body. Resistance, pressure, and flow measurements were taken at a fixed flow rate in the loop.

3.2. Experimental procedure

R-123 and de-ionized water were utilized as the working fluid in the experiments under exit pressures of 101–267 kPa at ambient inlet temperature. First, the flow rate was fixed at the desired value, and data was taken after a steady flow rate had been obtained, while exit pressure was kept constant. Prior to acquiring experimental data, the flow meter reading was adjusted to the desired flow rate. To obtain pressure data, voltage was applied in 0.5 V increments across the heater, and the current/voltage data was recorded while ensuring the constancy of the flow rate, and pressures at the inlet and exit ports of the micro-pin fin device were measured at each data point. From the heater, at each data point resistance values were also acquired. The same procedure was repeated for other flow rates.

The uncertainties of the measured values, which are provided in Table 2, were obtained from manufacturer's specification sheets, while the uncertainties of the derived parameters were calculated using the method developed by Kline and McClintock [26].

4. Signal processing

In order to reveal the differences in pressure drops before and after unstable boiling conditions, Discrete-Time Fourier Transforms (DFT) [27] of pressure fluctuations were taken.

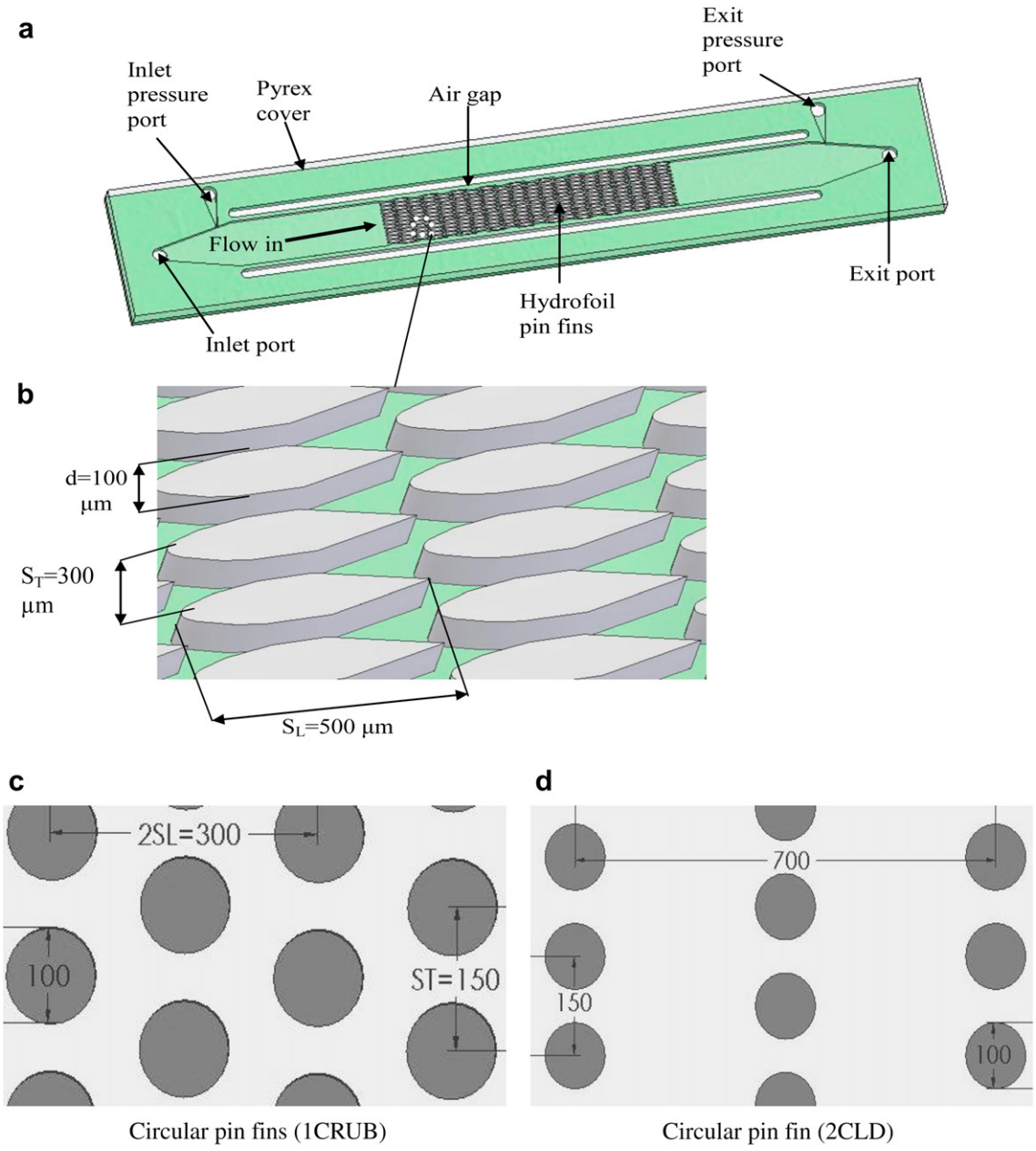

Fig. 1. (a) CAD model of the micro-pin fin heat sink (b) Zoom in to a micro-pin fin heat sink (3HWUB). Where d is chord thickness, S_T is transverse pitch and S_L is longitudinal pitch. (c) Other micro-pin fin heat sinks (1CRUB, 2CWUB).

Pressure drop is denoted as $x(t)$as a function of time, while $X(f)$ is its Fourier Transform of $x(t)$. If N measurements were taken uniformly in time with a period T_s then the measurement constitutes the following discrete-time sequence:

$$x[n] \equiv x(nT_s) \text{ for } n = 0, \ldots, N-1 \tag{1}$$

Table 1
Devices tested in the current study.

Device number	Working fluid	Pin shape	Pin configuration	Pin fin diameter/ chord thickness (μm)	S_T (μm)	S_L (μm)
1CRUB	R-123	Circular	Staggered	100	150	150
2CWUB	Water	Circular	Staggered	100	150	350
3HWUB	Water	Hydrofoil	Staggered	100	300	500

where n denotes the time index of the sample taken at $t = nT_s$, and T_s is sampling period in terms of s.

The N point DFT calculates the samples of the $X(f)$ determined at frequency $f = (k/N)(1/T_s)$for $k = 0, 1, \ldots, N-1$, which can be calculated as

$$X[k] = \sum_{n=0}^{N-1} x[n] e^{-j\frac{2\pi kn}{N}} \tag{2}$$

where $j \equiv \sqrt{-1}$, k is the index of the frequency domain sample taken at $f = (k/N)(1/T_s)$ and $X[k] \equiv X(f)|_{f=(k/N)(1/T_s)}$.

In practice, DFT in Eq. 2 can be implemented by using Fast-Fourier transform (FFT) [27]. In order to analyze the signal behavior before and after unstable boiling, FFT profiles of the signals are used to monitor their energy spreads over the frequency. For this

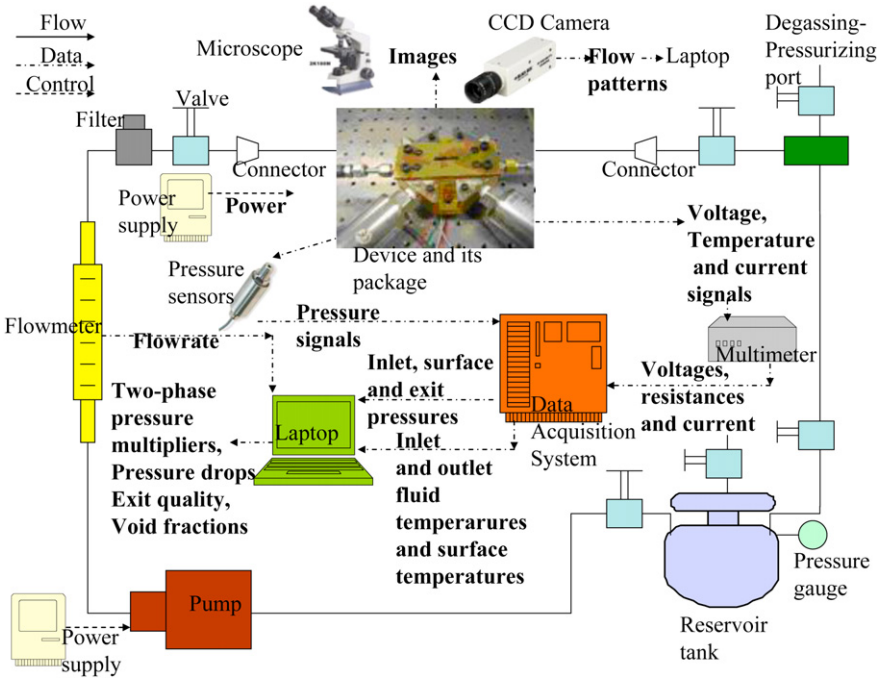

Fig. 2. Experimental setup.

analysis, FFT size N was taken as 2000, which corresponds to a frequency band of 500 Hz since the sampling periods between time domain samples were 10^{-3}s.

To quantify the change in the pressure signals initiation of unstable boiling, first the peak of the magnitude of the spectrum$X[k]$ is calculated for both before the unstable boiling and after the unstable boiling as

$$X_p = \max_{k=0,1,\ldots,N-1} |X[k]| \tag{3}$$

In addition to the peak of the magnitude spectrum, the mean of the magnitude spectrum on the side-lobes was also considered for each case. To perform this analysis, starting after W_1 frequency samples, the magnitude spectrum is windowed within a width of length W (width of sampling period in terms of s^{-1}) before and after the spectrum peak (Fig. 3). The spectrum samples within the prescribed window are named as side-lobe samples. Accordingly, the mean of the spectrum over the side-lobes can be calculated as

$$\overline{X}_s = \frac{1}{W} \sum_{k=W_1}^{W_1+W-1} |X[k]| \tag{4}$$

5. Results and discussion

5.1. Surface temperature curves

Fig. 4 displays the average surface temperature as a function of effective heat flux for Devices 1CRUB (Circular, R-123, Unstable, Boiling), 2CWUB (Circular, Water, Unstable, Boiling) and 3HWUB (Hydrofoil, Water, Unstable, Boiling). High mass velocities ($G > 300$ kg/m^{2}s) were deliberately chosen to check for the extent of the presence of unstable boiling. A typical linear $\overline{T}-q''$ curve is notable in the single-phase flow region, which is a characteristic feature of constant heat flux single-phase flow. Here $\overline{T}$is average surface temperature in terms of °C, $q''$is heat flux in terms of W/cm^2. As expected, a decrease is observed in the slope as the flow rate increases. For Device 1CRUB, the linear profile in the surface temperature maintains the same slope even considerably beyond the corresponding liquid saturation temperature. According to flow visualization, single-phase flow is observed beyond the saturation temperature, and no apparent phase change is noted. At a definite critical point, a meager increase in heat flux results in an abrupt and intense boiling with large fluctuations in the surface temperature, which is characterized as unstable boiling.

Table 2
Uncertainty data from the experiment.

Uncertainty	Error
Mass flux, G (for each reading)	1.0%
Pressure Readings (for the range)	0.25%
Ambient temperature	0.1 °C
Electrical power, P	0.7%
Average temperature, $\overline{T}$	0.5 °C

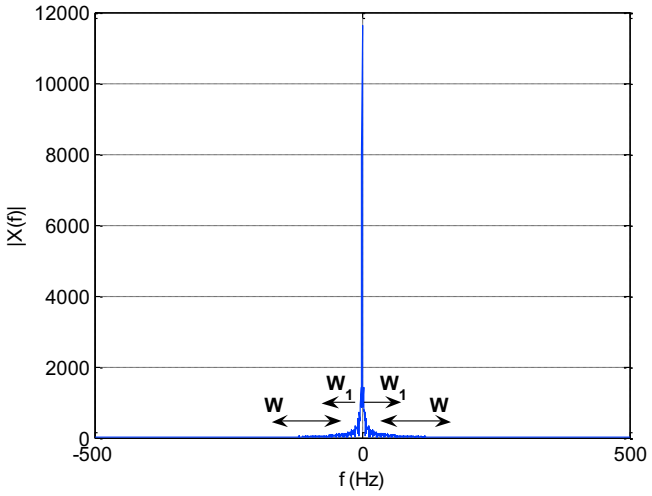

Fig. 3. W and W_1 displayed in a representative FFT profile (unstable boiling $G = 329$ kg/m^{2}s).

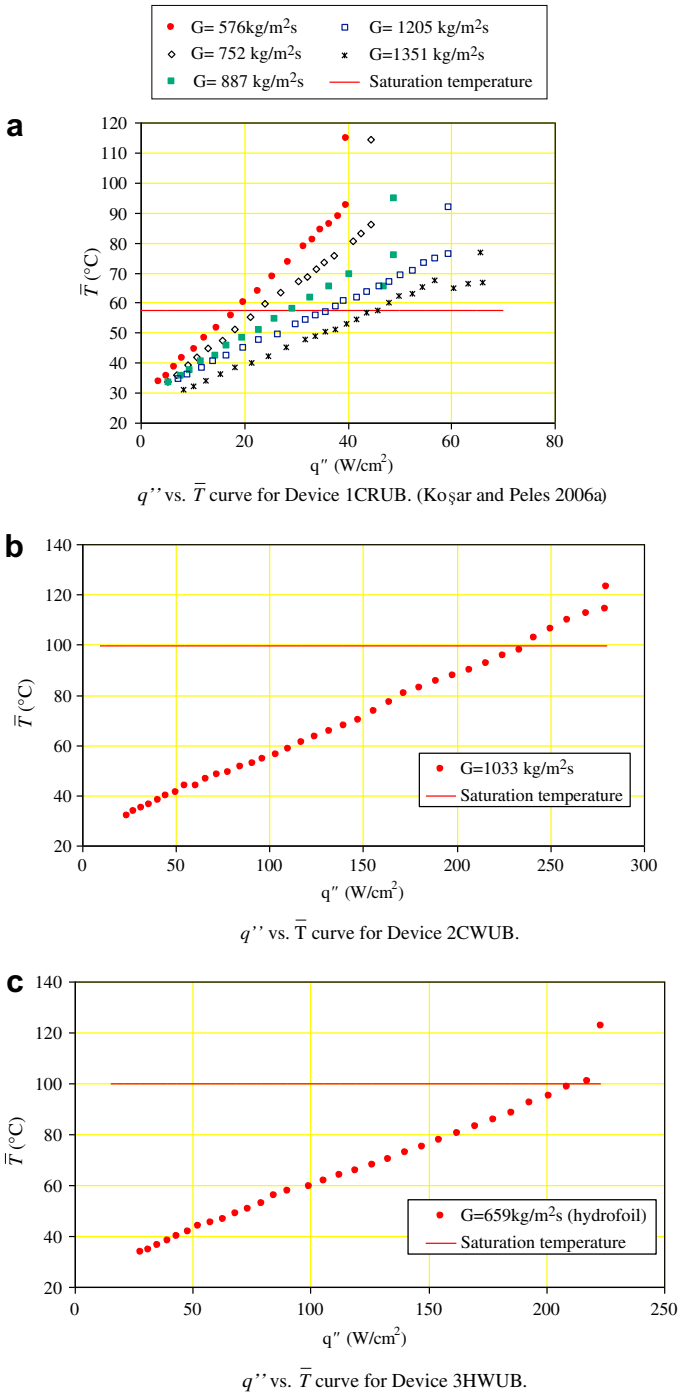

Fig. 4. q'' vs. $\overline{T}$curves. (a) q'' vs. $\overline{T}$curve for Device 1CRUB. (Kosar and Peles 2006a). (b) q'' vs. $\overline{T}$curve for Device 2CWUB. (c) q'' vs. $\overline{T}$curve for Device 3HWUB.

This trend is observed under all mass velocities with minor exceptions at $G = 887$ kg/m^{2}s and $G = 1351$ kg/m^{2}s, where a relatively short stable boiling region is detected. However, as heat flux is further increased, temperature fluctuations are inevitable.

As seen from Fig. 4 unstable boiling conditions are also present at boiling inception for Devices 2CWUB and 3HWUB; however, they occur at temperatures much closer to the saturation temperature compared to R-123 experiments on Device 1CRUB. The delay in boiling inception for Device 1CRUB is attributed to high wettability characteristics of R-123 and its tendency to fill large cavities available for nucleation increasing the superheat required for boiling inception. As a result, boiling inception is delayed to significantly higher surface temperatures than the saturation temperature of R-123.

To further distinguish between the boiling instability mechanisms in Device 1CRUB with R-123 and in Devices 2CWUB and 3HWUB with de-ionized water pressure drop characteristics are discussed in the next section.

5.2. Pressure drop

5.2.1. Pressure fluctuations

In devices and configurations leading to unstable boiling (1CRUB, 2CWUB, 3HWUB), a meager increase in heat flux triggers an intense boiling with considerable increase in the surface temperature marking the arrival of unstable boiling at boiling inception. Similarly, boiling conditions are typically accommodated with significant temperature and pressure drop oscillations in plain microchannels [4,6,21–23]. The unsteadiness of the pressure drop provides the basis to study the pressure fluctuations in micro-pin fin heat sinks.

Fig. 5a and b show the time dependence of pressure drop in Device 1CRUB at $G = 576$ kg/m^{2}s and $G = 887$ kg/m^{2}s immediately before unstable boiling begins, respectively. It can be noticed that there are no significant pressure fluctuations with respect to time averaged pressure drop ($\Delta p'_{max}$~0.5 kPa). This profile also prevails after unstable boiling initiates (Fig. 6a and b). As a result, peak to peak pressure drop fluctuations remain small compared to the time

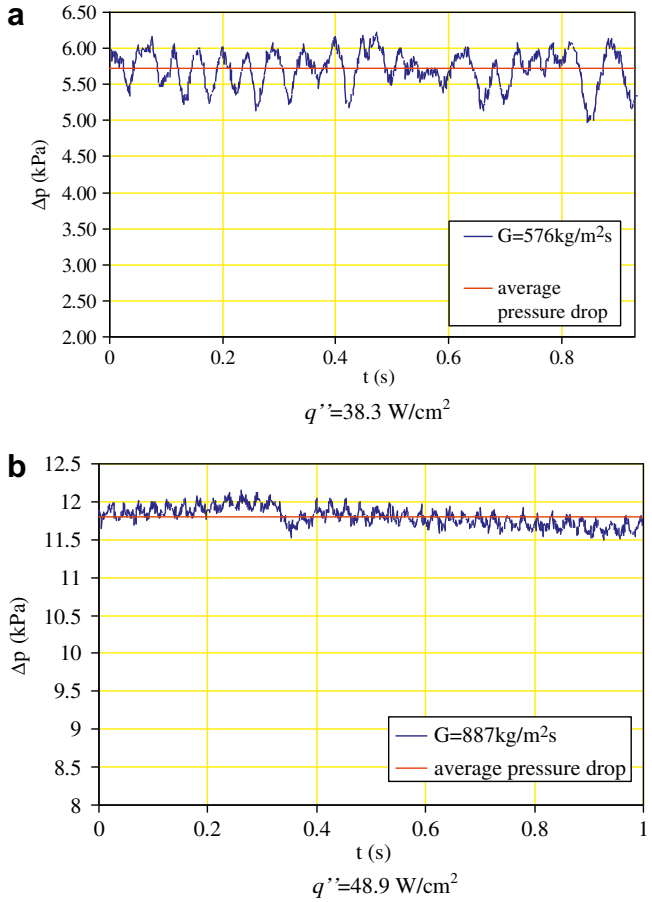

Fig. 5. Pressure fluctuations before unstable boiling conditions for Device 1CRUB at a) $G = 576$ kg/m^{2}s and b) $G = 887$ kg/m^{2}s.

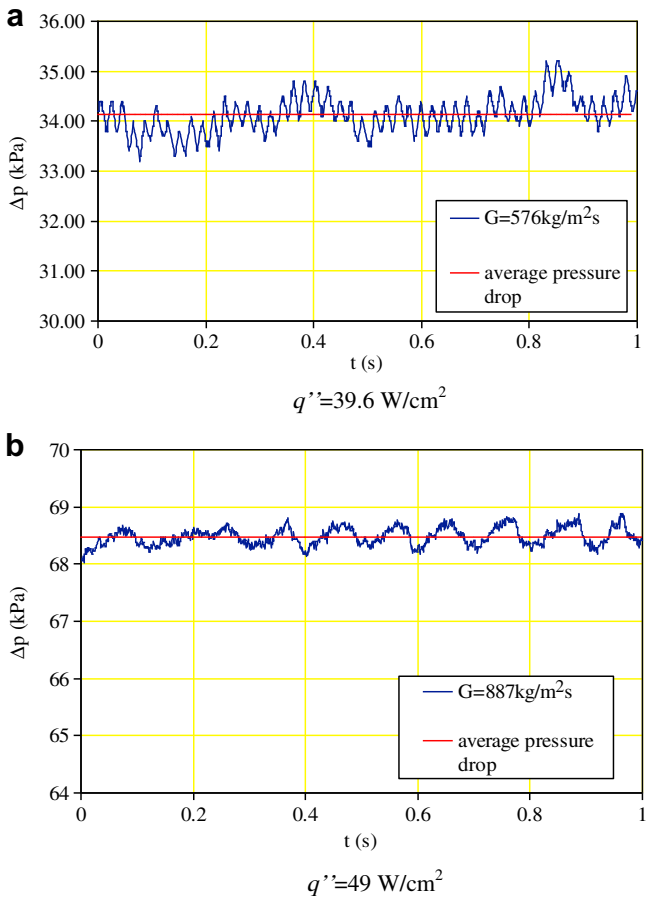

Fig. 6. Pressure fluctuations after unstable boiling conditions for Device 1CRUB at a) $G = 576$ kg/m^{2}s and b) $G = 887$ kg/m^{2}s.

averaged pressure drop before and after unstable boiling, which is in contrast to premature CHF condition and boiling instabilities in parallel microchannels, at which significant pressure fluctuations were reported in the literature [4,6,21–23].

In order to reveal the differences between pressure drop profile in unstable boiling and that in stable boiling, FFTs of pressure fluctuations are taken. In this technique, FFT profiles of the signals are used to analyze the signal behavior before and after unstable boiling and to identify their energy spreads over the frequency. From Fig. 7 it can be seen that the peaks of the spectrum increase by a factor of 5.43, 8.54 and 4.33 for $G = 329$, 576 and 887 kg/m^{2}s in Device 1CRUB, respectively. This clearly indicates a drastic change in the pressure signals with the initiation of unstable boiling and a resulting sharp increase in the energy peaks of the FFT profiles. Moreover, the mean of the magnitude spectrum on the side-lobes is also considered for each case. The ratios of the mean of the magnitude spectrum after unstable boiling to the mean of the magnitude spectrum before unstable boiling are calculated for $G = 329$, 576 and 887 kg/m^{2}s as 6.83, 6.38 and 4.28, respectively. These findings suggest that not only the spectrum peak increases significantly but the side-lobe energy also gets significantly higher after the inception of unstable boiling. It is important to note that the ratios of the spectrum peaks show more noticeable variations with mass velocity, whereas the ratios of the mean spectrum on side-lobes of unstable boiling to the mean spectrum on side-lobes stable boiling conditions vary less with mass velocity. As a result, because of its weaker dependence on mass velocity, the latter parameter can be considered as more reliable to determine the unstable boiling event for various mass velocities. This abrupt change in pressure drop signals complies with rapid bubble growth instability mechanism in microchannel systems, which was presented as a boiling instability mode by Kuo and Peles [24] and was characterized by high frequencies (f~100 Hz). This sort of boiling instabilities is particularly dominant at high superheat values for boiling inception and flow reversals due to high pressures with bubble growth. Since both of

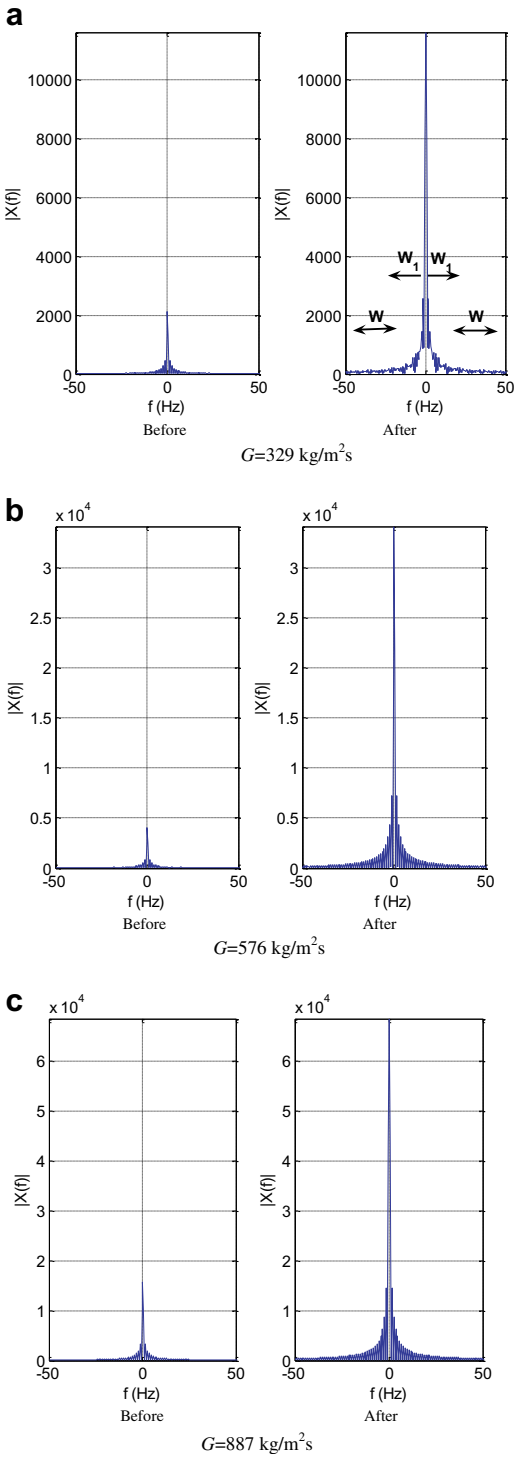

Fig. 7. FFT profiles before and after the unstable boiling.

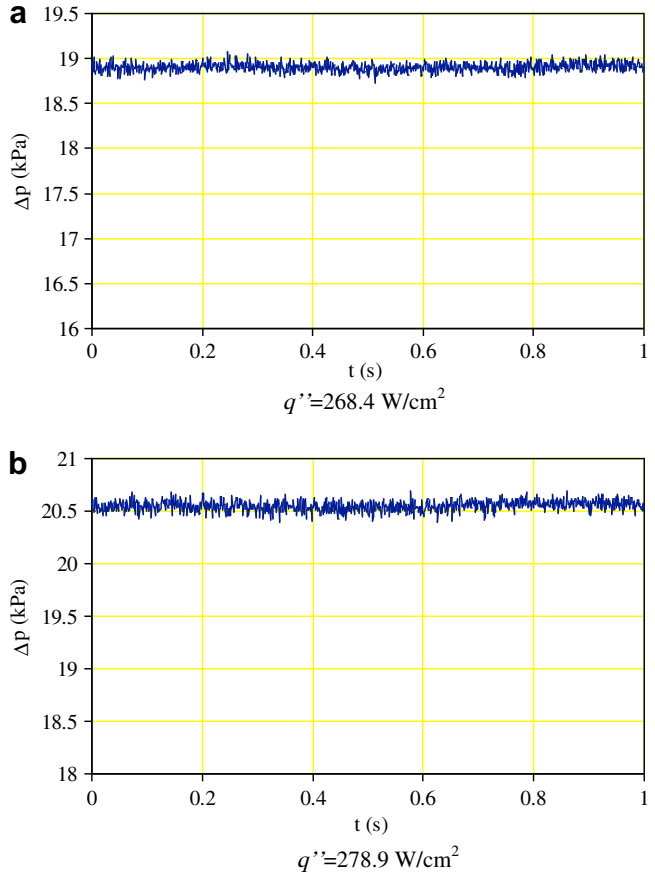

Fig. 8. Pressure fluctuations a) before and b) after unstable boiling conditions for Device 2CWUB at $G = 1033$ kg/m^{2}s.

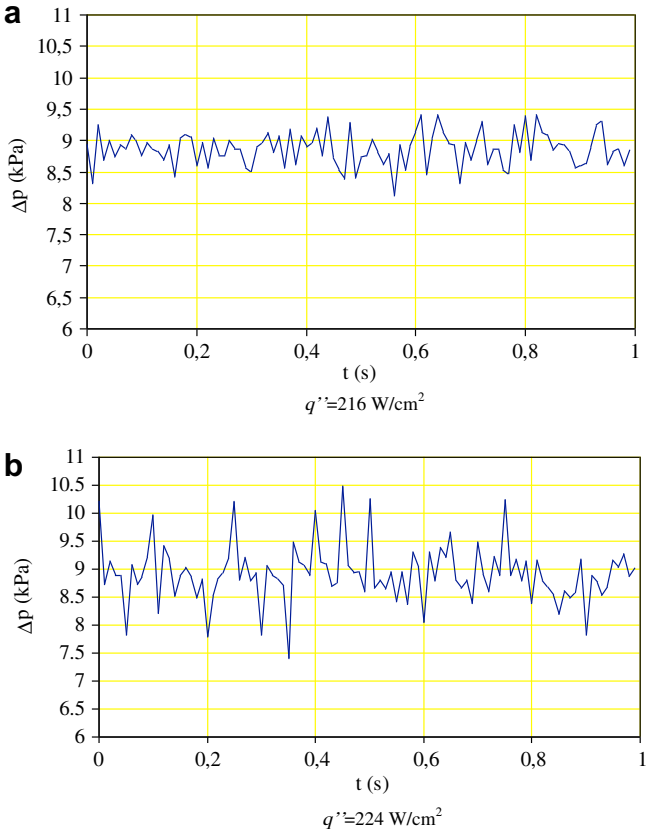

Fig. 9. Pressure fluctuations a) before and b) after unstable boiling conditions for Device 3HWUB at $G = 659$ kg/m^{2}s.

these conditions are present in experiments with the Device 1CRUB, and severe changes in pressure drop signals are recorded, the boiling instability mechanism leading to unstable boiling can be associated with rapid bubble growth.

The pressure fluctuations for Devices 2CWUB and 3HWUB are demonstrated in Fig. 8a and b, and Fig. 9a and b, respectively. As seen from these figures, pressure fluctuations are also minor with respect to average pressure drop in these devices. Moreover, it can be observed that the peaks of the spectrum increase by a factor of 1.0871 and 1.0059 for 2CWUB and 3HWUB, respectively (Figs. 10 and 11). Moreover, the means of the magnitude spectrum on the side-lobes are also obtained from these devices. The ratios of the mean of the magnitude spectrum after and before instability for Devices 2CWUB and 3HWUB are 1.0855 and 1.0065, respectively. As seen from these profiles, there is no significant change in pressure drop signals with the initiation of unstable boiling in Devices 2CWUB and 3HWUB unlike the pressure signals in Device 1CRUB operated with R-123. This suggests a different boiling instability mechanism. In the current configuration, there is a significant compressible upstream volume within the heated section due to the absence of inlet restriction [6,24] so that upstream compressible volume instability having low frequency (in flow and pressure fluctuations) nature is the dominant boiling instability mechanism in the Devices 2CWUB and 3HWUB (rather than the rapid bubble growth mechanism). The change in the mode of boiling instability in those devices is reflected as similar FFT profiles presented in Figs. 10 and 11.

5.2.2. Pressure drop demand curves

The dependence of the pressure drop on the effective heat flux provides a useful tool to predict boiling inception and CHF condition. It is well documented and explicated in literature that the pressure drop has a minimum at the onset of significant void (OSV) conditions, beyond which the bubbles detaching from the heated

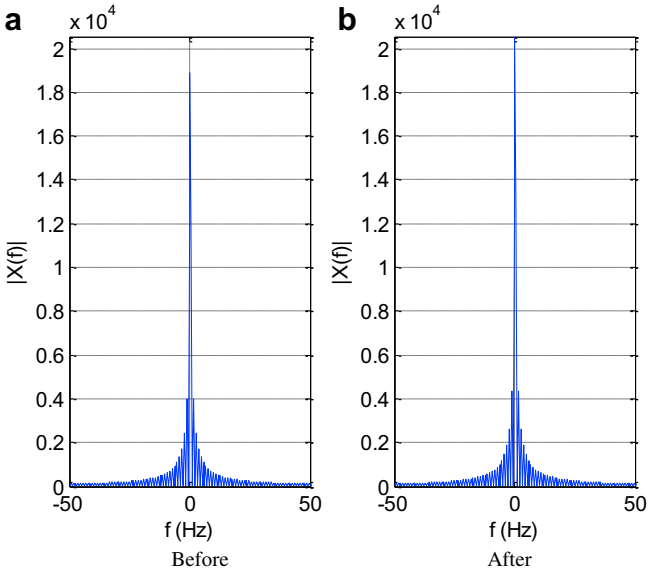

Fig. 10. FFT profile of pressure drop fluctuations before and after unstable boiling conditions for Device 2CWUB at $G = 1033$ kg/m^{2}s.

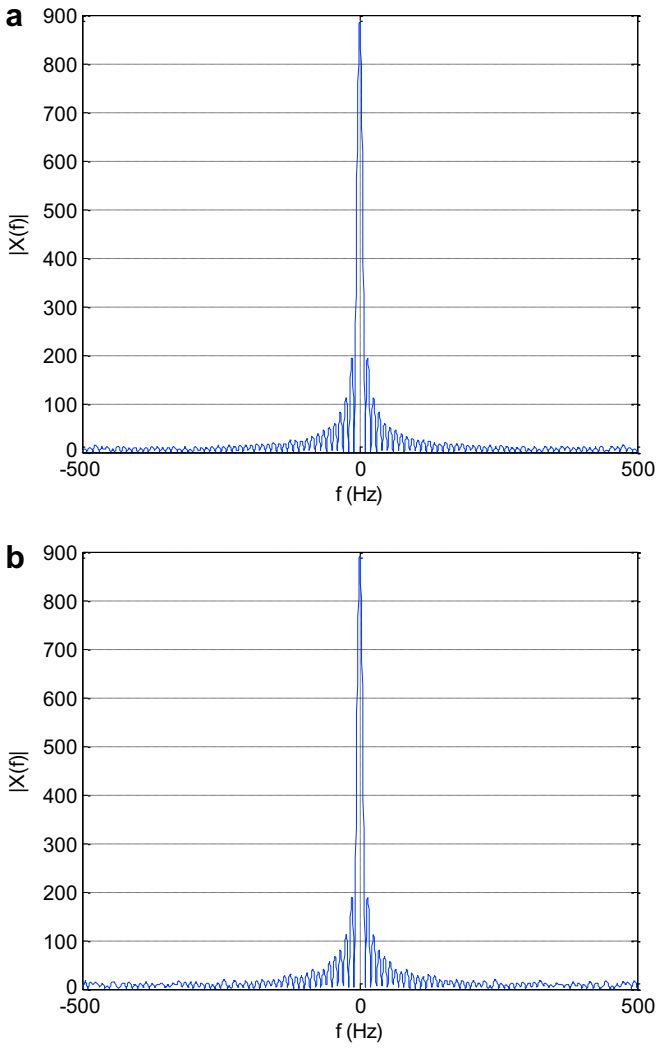

Fig. 11. FFT profile of pressure drop fluctuations a) before and b) after unstable boiling conditions for Device 3HWUB at $G = 659$ kg/m^{2}s.

channel wall can survive condensation sufficiently to cause bulk void [28]. An increase in heat flux beyond the OSV conditions results in an increase in the pressure-drop required to maintain a fixed flow rate.

Fig. 12 shows the characteristic pressure demand curves for Devices 1CRUB, 2CWUB and 3HWUB. The pressure drop demand for a fixed mass flux declines moderately with heat flux during the single-phase flow, since the liquid viscosity drops with the increase in liquid temperature during single-phase flows, which in turn has a decreasing effect on the required pressure drop to maintain a constant flow rate. The decline in pressure drop continues until the characteristic minimum is reached, and a surge in the void fraction takes place. Beyond this minimum, two-phase flow is observed, and the increase in the void fraction increases the pressure drop demand. The only difference in the profiles between refrigerant and water studies is the large jump in Device 1CRUB operated with R-123, whereas the jump is quite small for Devices 2CWUB and 3HWUB. This is attributed to the delay in boiling inception for Device 1CRUB due to high wettability of R-123 compared to water and also due to the rapid bubble growth instability mechanism. However, after this delay, a rigorous boiling occurs, which leads to a large pressure jump and high frequency fluctuations.

5.3. Flow visualization under unstable boiling conditions

To reveal other differences between unstable boiling with water and R-123, images of unstable boiling conditions are studied. Fig. 13 demonstrates periodic flow patterns of Device 1CRUB at $G = 887$ kg/m^{2}s. Fig. 13a corresponds to the initiation of boiling, when small bubbles start to develop. As time progresses, active nucleate site distribution intensifies particularly near the pin fin stagnation region, where there is no flow and therefore, a temperature rise occurs (Fig. 13b). Bubbles can clearly be seen in the inlet region on the first column of micro-pin fins. Bubbles appear on the surface of micro-pin fins as well as on the surface of the microchannel and coalesce to build vapor slugs, which propagate toward the inlet plenum (Fig. 13c and d). These slugs unite into a large slug occupying a significant portion of the inlet region of the device (Fig. 13e). The large slug is then pushed by the drag force against the surface tension forces

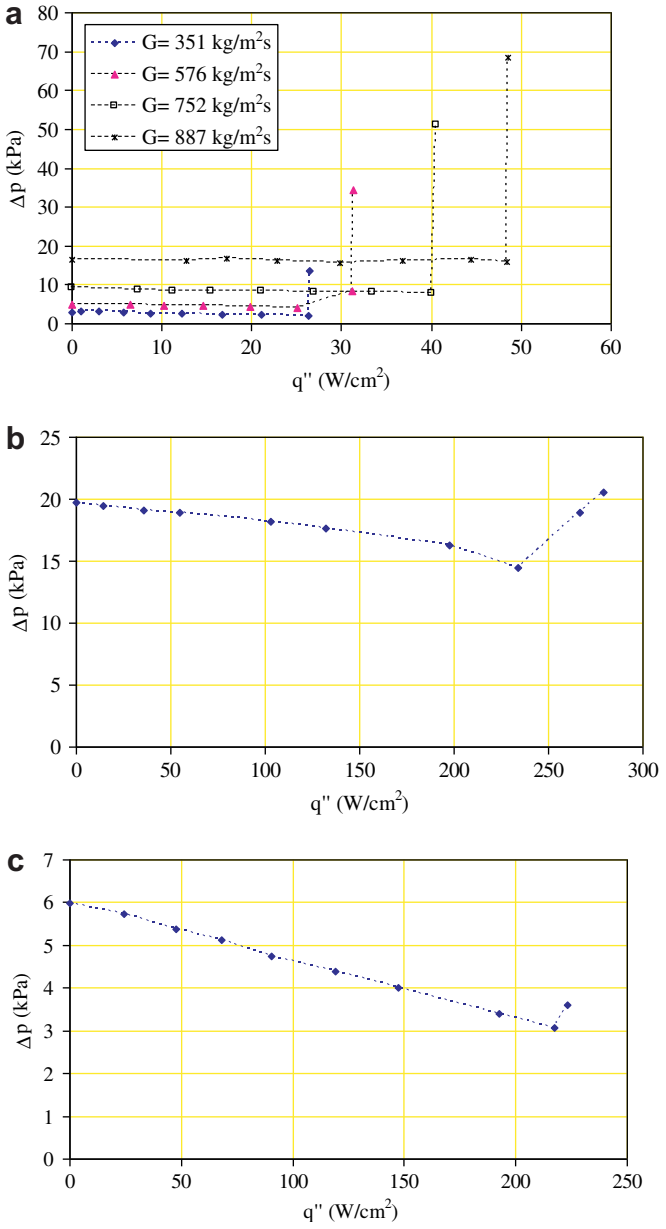

Fig. 12. Pressure drop demand curves for devices a) 1CRUB, b) 2CWUB and c) 3HWUB.

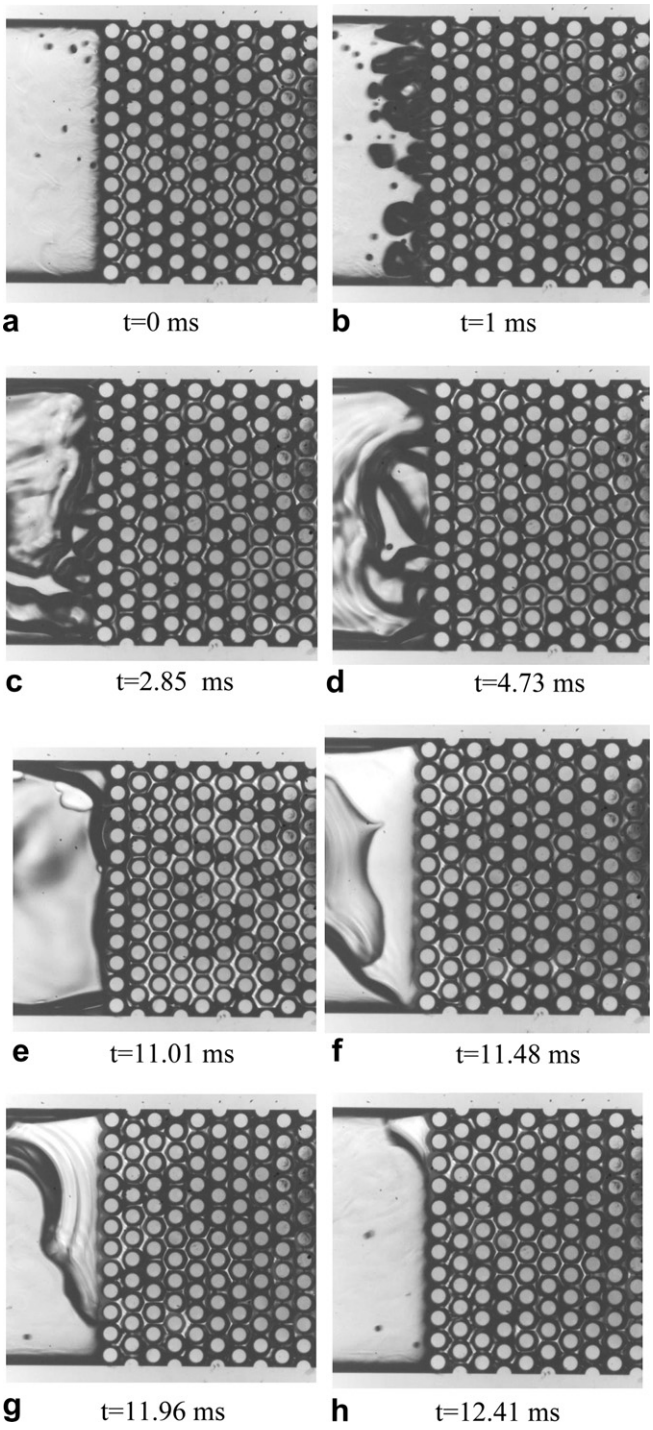

Fig. 13. Unstable boiling images recorded for Device 1CRUB (q'' = 39.6 W/cm^2 G = 576 kg/m^2).

acting on it (Fig. 13f–h), so that it collapses, and a two-phase mixture travels from the inlet region to the exit of the device. This sequence of events occurs periodically for all flow rates of Device 1CRUB. The major difference between the results for water and R-123 lies in the surface superheat temperature during boiling inception, which is much higher for the refrigerant. The main reason can be attributed to better wettability characteristics of R-123 so that all of the larger surface cavities are flooded and consequently a high superheat surface temperature is required for nucleation as discussed in the previous section. Once boiling incepts, a sudden appearance and rapid growth of the vapor phase in liquid were observed, and high values of superheat wave have been noted, which are typical of rapid bubble growth instability. The explosive vapor growth seems to be periodic in nature with respect to the visualization study (with a period of 12.41 ms), which is typical of rapid bubble growth mechanism. For water, however, no high superheats are required for boiling inception. After the formation of a large volume of slug in the inlet region (moving toward the inlet plenum of Device 2CWUB), the flow pushes the slug with much lower frequencies (~32 Hz) compared to the refrigerant boiling flow in Device 1CRUB (Fig. 14). The difference in the periods in flow patterns between water and R-123 may be linked to high surface tension forces of water, which provide resistance for bubbles to detach form pin fin surfaces and thus enable them to grow and merge to larger bubbles. The more space the bubbles occupy, the more likely the temperature concentration occurs, which results in a large rise in the average surface temperature. When the flow becomes able to force the slug along the device, liquid replenishment occurs along with a drop in the average surface temperature. As a result, the surface temperature shows a cyclic temperature profile with the cyclic occurrence of flow patterns. Much lower frequencies (20 Hz) in the occurrence of series of these flow patterns in water studies, which was also repeated for the device 3HWUB showing this characteristic for both circular and hydrofoil shaped pin fins, indicate a different boiling instability mechanism (upstream compressible volume instability) rather than rapid bubble growth instability observed in R-123.

6. Conclusions

Unstable boiling was studied in three different micro-pin fin heat sinks. Pressure signals and flow images were acquired under unstable boiling conditions, which were accompanied by severe temperature fluctuations. The main conclusions drawn from this study are:

- Similar to parallel microchannel array, flow instabilities are of concern during flow boiling in micro-pin fin heat sinks.
- Onset of boiling was accompanied by considerable flow instabilities in all the tested micro-pin fin heat sinks with a corresponding increase in surface temperature.
- For water, the magnitude of the pressure drop fluctuations before and after unstable boiling was not significant regardless the shape of the pin fin. Peak to peak pressure drop fluctuations remain small compared to the time averaged pressure drop for all the devices.
- For R-123, a drastic change is observed in the pressure signals with the initiation of unstable boiling, and a sharp increase in the magnitude peaks of the FFT profiles becomes apparent. Moreover, not only the spectrum peak increases significantly but the side-lobe energy also significantly increases after the inception of unstable boiling, which is an indicator of rapid bubble growth instability. For the devices operated with water (both circular and hydrofoil shaped micro-pin fin devices), no significant change is observed in the FFT profiles with unstable boiling. Upstream compressible volume instability rather than rapid bubble growth instability prevails under these unstable boiling conditions.
- The conclusions about the boiling instability mechanisms are supported by flow visualization. The recorded set of surface temperatures exhibit a cyclic temperature profile with the cyclic occurrence of flow patterns in all the devices following boiling inception. The high frequency of oscillations for the device operated with R-123 (~80 Hz) is in agreement with the frequency of the rapid bubble growth instabilities. For the devices operated with water, the periodic occurrence of flow

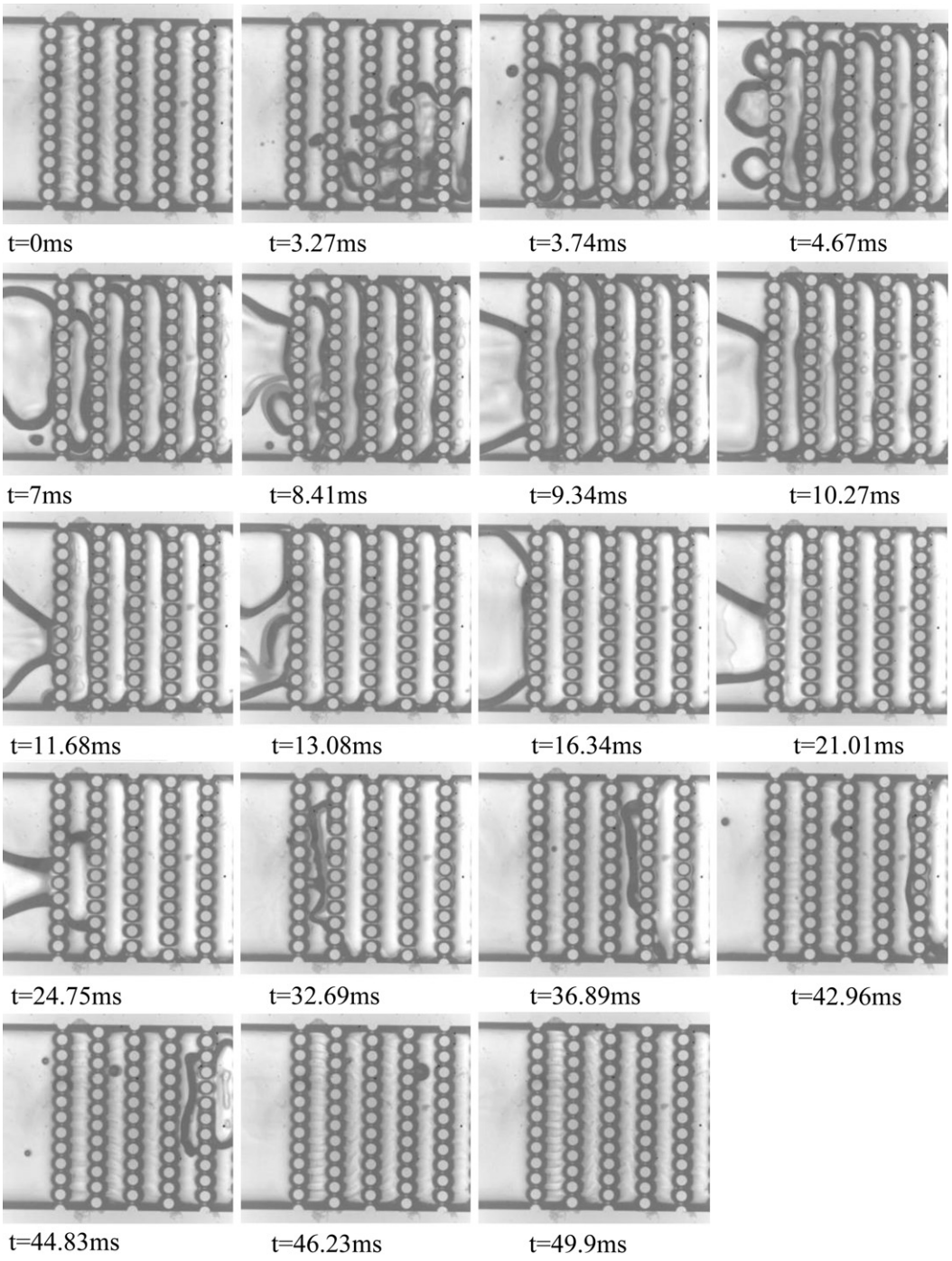

Fig. 14. Unstable boiling images recorded for Device 2CWUB ($q'' = 278.9$ W/cm^2 $G = 1033$ kg/m^2).

patterns becomes much less frequent (~20 Hz) regardless of the micro-pin fin structure, suggesting a different boiling instability mechanism (upstream compressible volume instability) of less frequent nature and without any high superheat requirement.

Acknowledgements

This work was supported by TUBITAK (The Scientific and Technological Research Council of Turkey) Support Program for Scientific and Technological Research Projects Grant, 107M514. Graduate student support provided by the Faculty of Engineering and Natural Sciences of Sabancı University is greatly appreciated.

References

[1] A.E. Bergles, J.H. Lienhard, G.E. Kendall, P. Griffith, Boiling and evaporation in small diameter channels. Heat Transfer Engineering 24 (2003) 18–40.
[2] S.V. Garimella, V. Singhal, Single-phase flow and heat transport and pumping considerations in microchannel heat sinks. Heat Transfer Engineering 25 (2004) 15–25.
[3] S.G. Kandlikar, W.J. Grande, Evaluation of single-phase flow in microchannels for high heat flux chip cooling – thermohydraulic performance enhancement and fabrication technology. Journal of Heat Transfer Engineering 25 (2004) 5–16.
[4] S.G. Kandlikar, Heat transfer mechanisms during flow boiling in microchannels. Journal of Heat Transfer 126 (2004) 8–16.
[5] J.R. Thome, Boiling in micro channels: a review of experiment and theory. International Journal of Heat and Fluid Flow 25 (2004) 128–139.

[6] A.E. Bergles, S.G. Kandlikar, On the nature of critical heat flux in microchannels. Journal of Heat Transfer 127 (2005) 101–107.
[7] B. Agostini, M. Fabbri, J.E. Park, L. Wojtan, J.-R. Thome, B. Michel, State of the art of high heat flux cooling technologies. Heat Transfer Engineering 28 (2007) 258–281.
[8] Y. Peles, C.-J. Kuo, A. Koşar, C. Mishra, B. Schneider, Forced convective heat transfer across a pin fin micro heat exchanger. International Journal of Heat and Mass Transfer 48 (2005) 3615–3627.
[9] A. Koşar, C. Mishra, Y. Peles, Laminar flow across a bank of low aspect ratio micro pin fins. Journal of Fluids Engineering 127 (2005) 419–430.
[10] E.G. Colgan, B. Furman, M. Gaynes, W. Graham, N. LaBianca, J.H. Magerlein, R.J. Polastre, M.B. Rothwell, R.J. Bezama, R. Choudhary, K. Marston, H. Toy, J. Wakil, J. Zitz, R. Schmidt, A practical implementation of silicon microchannel coolers for high power chips, in: 21st IEEE SEMI-THERM Symposium, San Jose, CA, March 15–17, 2005.
[11] A. Koşar, Y. Peles, Convective flow of refrigerant (R-123) across a bank of micro pin fins. International Journal of Heat and Mass Transfer 49 (2006) 3142–3155.
[12] A. Koşar, Y. Peles, Thermal-hydraulic performance of MEMS-based pin fin heat sink. Journal of Heat Transfer 128 (2006) 121–131.
[13] A.M. Siu-Ho, W. Qu, F.E. Pfefferkorn, Experimental study of pressure drop and heat transfer in a single-phase micro-pin-fin heat sink. ASME Journal of Electronic Packaging 129 (2007) 479–487.
[14] A. Koşar, Y. Peles, Boiling heat transfer in a hydrofoil-based micro pin fin heat sink. International Journal of Heat and Mass Transfer 50 (2007) 1018–1034.
[15] R.S. Prasher, J. Dirner, J.-Y. Chang, A. Myers, D. Chau, D. He, S. Prstic, Nusselt number and friction factor of staggered arrays of low aspect ratio micro pin fins under cross flow. Journal of Heat Transfer 129 (2007) 141–153.
[16] S. Krishnamurthy, Y. Peles, Gas-liquid two-phase flow across a bank of micro pillars. Physics of Fluids 19 (2007) 043302–04330214.
[17] S. Krishnamurthy, Y. Peles, Flow boiling of water in a circular staggered micro-pin fin heat sink. International Journal of Heat and Mass Transfer 51 (2008) 1349–1364.
[18] W. Qu, A. Siu-Ho, Liquid single-phase flow in an array of micro-pin-fins: Part I. Heat transfer characteristics. Journal of Heat Transfer 130 (2008) 1224021–12240211.
[19] W. Qu, A. Siu-Ho, Liquid single-phase flow in an array of micro-pin-fins: Part II. Pressure drop characteristics. Journal of Heat Transfer 130 (2008) 124501.
[20] C.A. Konishi, W. Qu, F.E. Pfefferkorn, Experimental study of water liquid-vapor two-phase pressure drop across an array of staggered micropin-fins. Journal of Electronic Packaging 131 (2009) 021010.1–021010.8.
[21] W. Qu, I. Mudawar, Measurement and prediction of pressure drop in two-phase micro-channel heat sinks. International Journal of Heat and Mass Transfer 46 (2003) 2737–2753.
[22] S.G. Kandlikar, W.K. Kuan, D.A. Willistein, J. Borrelli, Stabilization of flow boiling in microchannels using pressure drop elements and fabricated nucleation sites. Journal of Heat Transfer 128 (2006) 389–396.
[23] A. Koşar, C.J. Kuo, Y. Peles, Suppression of boiling flow oscillations in parallel microchannels with inlet restrictors. Journal of Heat Transfer 128 (2006) 251–260.
[24] C.J. Kuo, Y. Peles, Flow boiling instabilities in microchannels and means for mitigation by reentrant cavities. Journal of Heat Transfer 130 (2008) 072402.
[25] C.J. Kuo, Y. Peles, Pressure effects on flow boiling instabilities in parallel microchannels. International Journal of Heat and Mass Transfer 52 (2009) 271–280.
[26] S. Kline, F.A. McClintock, Describing uncertainties in single-sample experiments. Mechanical Engineering 75 (1953) 3–8.
[27] A.V. Oppenheim, R.W. Schafer, Discrete-time Signal Processing, second ed. Prentice Hall Signal Processing Series, 1999.
[28] J.G. Collier, J.R. Thome, Convective Boiling and Condensation, third ed.. Oxford University Press, Oxford, 1994.